Metalurgi (2024) 3: 141-150

METALURGI
Majalah Ilmu dan Teknologi
p-ISSN 0126-3188 | e-ISSN 2443-3926
ejurnalmaterialmetalurgi.lipi.go.id

CORROSION BEHAVIOR OF EQUIATOMIC BIO-HIGH ENTROPY ALLOYS CoCrMoMnNb FABRICATED IN MULTIPLE REMELTING PROCESSES

Fendy Rokhmanto[a, b, *], Aprilia Erryani[a, b], Albertus Deny Heri Setyawan[b], Yudi Nugraha Thaha[b], Ahmad Zakiyuddin[a], Ika Kartika[b], Sri Harjanto[a,*]

[a]Department of Metallurgical and Materials Engineering, University of Indonesia
Kampus UI, Kukusan, Depok, Indonesia 16424
[b]Research Center for Metallurgy, National Research and Innovation Agency (BRIN)
B.J. Habibie Sains and Technology Area, Banten, Indonesia 15314
*E-mail: fend001@brin.go.id; sri.harjanto@ui.ac.id

Received: 27-10-2025, Revised: 05-01-2026, Accepted: 07-01-2026

Abstract

High-entropy alloys are described as equiatomic alloys of more than five elements or materials with five or more element constituents with a high mixing entropy (ΔSmix ≥ 1.5R), where the composition of the element is 5–35%, respectively. One application of HEA (high entropy alloys) materials is in the orthopedic field, where they are developed as biomaterials. Behavior, the correlation between the elemental distribution, and the microstructure of the material were investigated during multiple remelting processes known as Bio-HEAs. The development of Bio-HEAs is exciting in terms of design material, fabrication, and their properties. In this paper, the corrosion behavior and the correlation of the elemental distribution and the microstructure of the material were investigated during the multiple remelting process. The equiatomic CoCrMoMnNb was prepared in vacuum arc melting under an argon atmosphere and melted in a water-cooled copper mold. The total amount of ingot was approximately 25 grams, then flipped and remelted several times, 4, 8, and 12 cycles. The final composition of the alloys was confirmed by EDX (energy dispersive x-ray spectroscopy). The microstructure was investigated with an optical microscope and the SEM (scanning electron microscope). The corrosion parameter occurred in Hank's solution at 37°C, at a scan rate of 1 mV/s. The CCM-MnNb fabricated with 8 cycles of the remelting process exhibits the lowest corrosion rate (0.0038 mmpy) and donor densities (2.67 × 10^{19} cm^{-3}), while the charge transfer resistance number is the highest (18250.94 Ω cm^{-2}). The outstanding corrosion resistance of the alloys is induced by the presence of the finer dendrites and the chromium oxide (Cr_2O_3) protective layer on the alloy's surface.

Keywords: *High entropy alloy, bio-HEA, CoCrMo, biomaterial, remelting cycles, corrosion resistance*

1. INTRODUCTION

High entropy alloys (HEA) are described as equiatomic alloys of more than five elements or materials with five or more element constituents with a high mixing entropy (ΔSmix ≥ 1.5R), and the composition of the element is 5-35%, respectively [1]-[4]. The high entropy alloy material was introduced in 2004. Brian Cantor developed the equiatomic CrMnFeCoNi [5], and then, nowadays, known as the Cantor alloy. In its development up to 2016, 408 types of alloys with various applications have been obtained, which were then classified by D. B. Miracle and O. N. Senkov into 7 groups, that called as a taxonomy of HEA, there are: 3d transition HEA (Al, Co, Cr, Cu, Fe, Mn, Ni, Ti, V), Refractory HEA (Cr, Hf, Mo, Nb, Ta, Ti, V, W, Zr), Light metal HEA (Al, Be, Li, Mg, Sc, Si, Sn, Ti, Zn), Lanthanide (4f) transition metal HEA (Dy, Gd, Lu, Tb Tm, Y), Brass and bronze HEA (Al, Cu, Mn, Ni, Sn, Zn), Precious metal HEA (Ag, Au, Co, Cr, Cu, Ni, Pd,

DOI: 10.55981/metalurgi.2024.782

Metalurgi is Sinta 2 Journal (https://sinta.kemdikbud.go.id/journals/profile/3708) accredited by Ministry of Education, Culture, Research, and Technology, Republic Indonesia

Pt, Rh, Ru), and Interstitial compound HEA (with B, C, or N addition on the 3d HEA) [3].

One of the applications of HEA material is in the orthopedic field; the HEA material, which is developed as a biomaterial, is then known as Bio-HEAs. Bio-HEAs were introduced by Mitsuharu Todai et al. [6] and Shao Ping Wang et al. [7] in 2017, they developed equiatomic TiNbTaZrMo. In its development, the TiNbTaZrMo, TiZrHfNbTa, TiZrHfNbTaMo, TiZrHfCrMo, TiZrHfCoCrMo, and TiZrNbTaFe were introduced as Bio-HEA [6]-[17], Takeshi Nagase et al. [18] Introduced "CCM base Bio-HEA" in 2019, the alloys are CoCrMoFeMn, CoCrMoFeMnW, and CoCrMoFeMnWAg . Alina Elena Bololoi et al. [19] introduced CoCrMoNbTi as a CCM base Bio-HEA in 2023 by powder metallurgy process. Meanwhile, in 2017, Mina Zhang et al. [20] developed CoCrMoNbTi as a refractory HEA, the composition ratio of CoCrMo is more than 50%, so it can be classified as a CCM base Bio-HEA.

The development of Bio-HEAs is exciting both in terms of design material, fabrication, and their properties. The material design must follow several rules; the entropy is more than 12.471 J/K mol ($\Delta Smix \geq 1.5R$), the enthalpy is $-20 \leq \Delta Hmix \leq 5$ KJ/mol, the delta (δ) parameter is less than ≤ 6.6, the omega (Ω) parameter is greater than ≥ 1.1 [3], that mathematically can be described with the following equation:

$$\Delta Smix = -R \sum_{i=1}^{n} xilnxi \quad (1)$$

$$\Delta Hmix = \sum_{i=1,\, i\neq j}^{n} 4\Delta Hijxixj \quad (2)$$

$$\delta = 100\sqrt{\sum_{i=1}^{n} xi\left(1-\frac{ri}{\bar{r}}\right)^2} \quad (3)$$

$$\Omega = \left|\frac{Tm\,\Delta Smix}{\Delta Hmix}\right| \quad (4)$$

$$Tm = \sum_{i=1}^{n} xi(Tm)i \quad (5)$$

Where the ΔHij is the mixing enthalpy of two elements, ri is the atomic radius of the element, $\hat{r}$ is the average atomic radius of the alloy, and Tm is the melting temperature.

The biocompatibility of the Bio-HEA became crucial during material design. Biocompatibility can be analyzed by studying corrosion behavior in the simulated body fluids. Recently, the fabrication of Bio-HEAs has been dominated by the casting process in the vacuum arc melting furnace [6]-[7],[9],[13],[15],[17]-[18],[20], where the ingots are melted several times to improve the homogeneity of the alloying elements that relate to the mechanical properties and corrosion resistance of the alloys. The remelting cycles vary; several of them are remelted from 5 to 10 times, and most are remelted more than 10 times, though specific numbers are not stated. Based on that data, it is not possible to determine the optimal cycle times of the remelting process.

However, despite the application of multiple remelting cycles in Bio-HEA fabrication being commonly used, the influence of the number of remelting cycles on microstructure uniformity and corrosion resistance has not been systematically evaluated. Therefore, in this paper, the correlation of the corrosion behavior, elemental distribution, and microstructure of the material will be investigated during the multiple remelting processes. The developed material is equiatomic CCM base Bio-HEA CoCrMoMnNb, which refers to the traditional CoCrMo implant material, which is one of the biomaterials with good corrosion resistance and high wear resistance, making it suitable for orthopedic implants.

2. MATERIALS AND METHODS

The equiatomic CoCrMoMnNb, constructed according to the high entropy alloys rules in equations 1–5, has ΔSmix: 13.38 J/K mol, ΔHmix: -8.64 J/K mol, Ω: 3.19, δ: 5.94, and Tm: 2060.8 K. The ingot was prepared in vacuum arc melting under an argon atmosphere; the raw material, cobalt and chromium lumps, molybdenum and titanium rods, and manganese flakes (99.9%) were melted in a water-cooled copper mold. The total amount of ingot was approximately 25 grams, then flipped and remelted several times, 4, 8, and 12 cycles. The final composition and microstructure of the ingots were examined by EDX (energy-dispersive x-ray spectroscopy) and SEM (scanning electron microscopy) JEOL 6390A, respectively. Samples were prepared with methanol, 10% HCl, and electroetched after polishing with alumina. The corrosion characteristics were evaluated by potentiodynamic polarization and EIS (electrochemical impedance spectroscopy) using an Autolab 302 Multi BA electrochemical working station with Hank's solution at 37 °C and a scan rate of 1 mV/s. The samples were prepared in a 1 cm^2 area and then sanded up to 1200-grade sandpaper.

3. RESULTS AND DISCUSSION

Table 1 presents the high entropy alloys parameter of the CCM-MnNb; the mixing entropy of the alloys in the various remelting processes is above 1.5R.

Table 1. High entropy alloy parameter after alloying

	ΔSmix (J/K mol)	ΔHmix (J/K mol)	Ω	δ	ρ	Tm (K)
MnNb 4	13.21	-9.04	3.16	5.39	8.46	2161.91
MnNb 8	12.96	-9.84	3.01	5.54	8.65	2288.73
MnNb 12	12.76	-10.48	2.82	5.53	8.75	2312.17

The data in Table 1 indicates that the CCM-MnNb alloys were still categorized as high entropy alloy material, although the presence of Mn increased up to 6.7% in the 12 cycle times, as shown in Table 2.

Table 2. SEM EDX composition after alloying (at. %)

	Co	Cr	Mo	Mn	Nb
MnNb 4	26.46 ± 1.2	22.80 ± 0.7	14.22 ± 2.4	18.31 ± 1.4	18.21 ± 2.9
MnNb 8	25.02 ± 3.5	24.16 ± 1.2	21.05 ± 6.3	9.12 ± 2.1	20.80 ± 2.1
MnNb 12	26.79 ± 4.9	21.4 1± 1.8	24.15 ± 7.8	6.70 ± 1.1	20.95 ± 1.8

Table 2 presents the average chemical composition (at. %) of the various spots on the matrix and dendritic area of the CCM-MnNb button ingot with EDX characterization. The data in Table 2 shows that the remelting process decreases manganese (Mn) concentration from 20% (at. %) to 18.31% in 4 cycle times, 9.12% in 8 cycle times, and 6.7% in 12 cycle times. The Mn loss during the remelting process is caused by the volatilization behavior of manganese, where the higher melting temperature and longer processing time will increase manganese volatization [21].

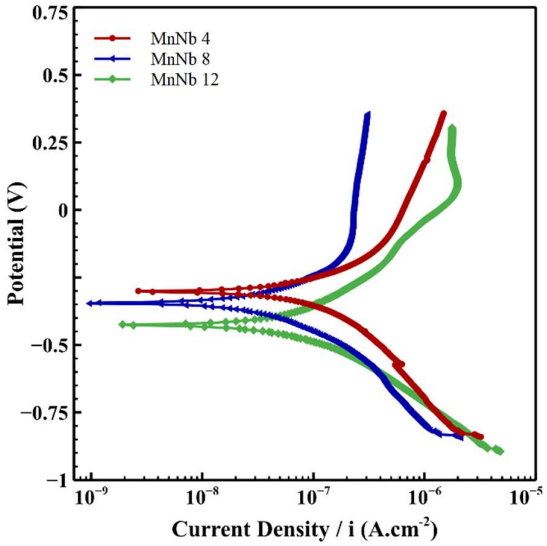

Figure 1. Tafel polarization curve of equiatomic CCM-MnNb, recorded at a scan rate of 1 mV/s, immersed in Hank's at 37 °C

The cycle of the remelting process induced the corrosion behavior of CCM-MnNb, as indicated by the shifting of the Tafel polarization curve of CCM-MnNb in Fig. 1. Meanwhile, Table 3 presents the potentiodynamic parameters of CCM-MnNb: corrosion current density, corrosion potential, and corrosion rate, which were calculated by Tafel extrapolation and included several biomaterials and Bio-HEAs (316L SS, CCM F75, TiAlV, and Bio-HEA TiZrNbTaMo).

Figure 1 shows that the corrosion potential shifts down up to -426 mV and the current density shifts left up to 0.94 μA/cm² after 12 cycles of remelting. A bigger current density indicates that the alloys are more corroded, which means they have weak corrosion resistance. In Table 3, the corrosion rate of CCM-MnNb 12 (0.0058 mmpy) is bigger than the others, CCM-MnNb 4 (0.0051 mmpy) and CCM-MnNb 8 (0.0038 mmpy). Compared to traditional biomaterials, Bio-HEAs have higher corrosion resistance, as shown in Table 3. The Titanium Bio-HEA TiZrNbTaMo has a lower corrosion current density than the Ti6Al4V. The CCM-MnNb 8 has a lower corrosion rate and a current density than CoCrMo F75, although it is higher than that of Titanium Bio-HEA.

Table 3. Potentiodynamic parameters of various alloys, immersed in Hank's at 37 °C

Alloys	i_{corr} (μA/cm²)	E_{corr} (mV)	Corr. Rate (mmpy)	Reff
316L SS	1.384	- 373	0.0109	[22]
CoCrMo F75	0.768	- 660	0.0061	[22]
Ti6Al4V	0.07	- 325	-	[23]
Bio-HEA TiZrNbTaMo	0.08	- 660	-	[23]
MnNb 4	0.828	- 302.28	0.0051	Present work
MnNb 8	0.619	- 345.88	0.0038	Present work
MnNb 12	0.940	- 426.22	0.0058	Present work

In this study, the CCM-MnNb 8 has a lower corrosion rate and a current density, which means it has higher corrosion resistance than others, even including the traditional CCM biomaterial (CoCrMo F75). The high corrosion resistance performance of CCM-MnNb alloys is related to the homogeneity of the elemental distribution, which is shown in the EDX characterizations in Figs. 2 and 3.

Figure 2 presents the EDX mapping of the alloys, while Fig. 3 shows the chemical composition of the CCM-MnNb matrix, as investigated using EDX point characterization. Figures 2 and 3 show that the matrix of CCM-MnNb dominates with cobalt, chromium, and manganese, even though molybdenum and niobium were also present. Meanwhile, the dendritic arm is rich in molybdenum and niobium, where it is typically an HEA material; the elements with high melting temperatures dominate in the dendritic arms [6]-[7].

Figure 2(a) shows the EDX mapping of the 4-cycle remelting process; the dendritic region appears dominated by Mo and Nb, while the other elements are widely spread on the matrix. Figure

3(a) reveals the dominance of Co (28.1%), Cr (23.4%), and Mn (19.9%). Whereas, the chromium induced the formation of a protective chromium oxide (Cr_2O_3) layer on the surface of Co-Cr alloys, which can protect from chloride ion attack [24]-[26]. Figure 2(b) reveals the EDX mapping of the 8-cycle remelting process, where the Co matrix is rich in Cr (25.7%), Mo (13.2%), and Nb (20.9%), as shown in Fig. 3(b), which enhances corrosion resistance. Mo and Nb are well known to have good compatibility [27]-[28], which can enhance the protection from chloride ion attack. Meanwhile, the Nb enrichment on the matrix is induced by the volatilization of Mn, where it decreases to 11.4% as shown in Fig. 3(b).

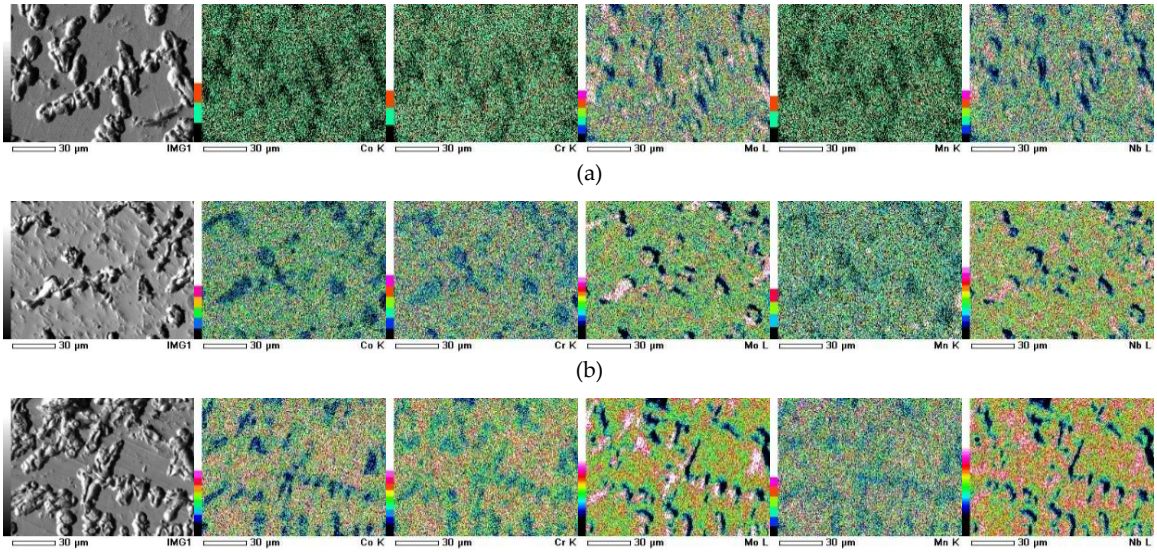

Figure 2. EDX – mapping image of equiatomic CCM-MnNb; (a) MnNb 4, (b) MnNb 8, (c) MnNb 12

Figure 2(c) shows the EDX mapping of the 12-cycle remelting process; the dendrite structure is observable and rich in Mo and Nb, and the Mn concentration decreased up to 7.16% as shown in Fig. 3(c). The Mn volatilization enhanced the homogeneous distribution of Nb (26.5%) in the matrix along with Co (31.5). The decrease of Mo (11.8%) and Cr (23.2%) content, as shown in Fig. 3(c), induces a lack of a Cr_2O_3 passive layer, which decreases the corrosion resistance, resulting in the highest corrosion rate (0.0058 mmpy).

CCM-MnNb 8 has the highest charge transfer resistance, as shown in the Nyquist plot in Fig. 4(a), which indicates that the alloys are strongly covered by a thin passive layer, which is Cr_2O_3 that protects from corrosion attack. CCM-MnNb 8 is also a higher impedance, as shown in Fig. 4(b). The Bode modulus plots show that in the high-frequency region (> 100 Hz), the $|Z|$ tends to remain constant and independent of frequency, and the low-frequency region has a linear relation with the impedance value, which means that the alloy has good protection from corrosion, which is chloride ion attack. Figure 4(c) is the Bode phase plot; the high and wide phase angle indicates the ideal capacitive behavior of alloys, and the CCM-MnNb has the biggest, which clarifies that the alloy has the best corrosion resistance.

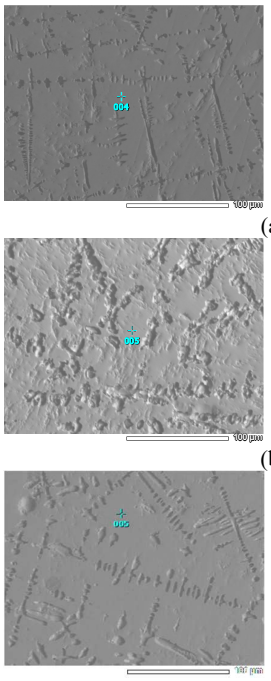

(a)

Element	Atomic %
Co	28.07
Cr	23.37
Mo	13.71
Mn	19.93
Nb	14.92

(b)

Element	Atomic %
Co	28.78
Cr	25.69
Mo	13.22
Mn	11.4
Nb	20.91

(c)

Element	Atomic %
Co	31.46
Cr	23.16
Mo	11.76
Mn	7.16
Nb	26.46

Figure 3. EDX – point Image of equiatomic CCM-MnNb; (a) MnNb 4, (b) MnNb 8, (c) MnNb 12

Figure 4(d) is the equivalent circuit model that was constructed based on the fitting result of impedance, and Table 4 is the fitting parameters of the equivalent circuit. The highest Rct (charge transfer resistance) on the CCM-MnNb indicates that the ion transfer between the alloy surface and the Hank's solution became tougher, which means the alloy has good corrosion resistance.

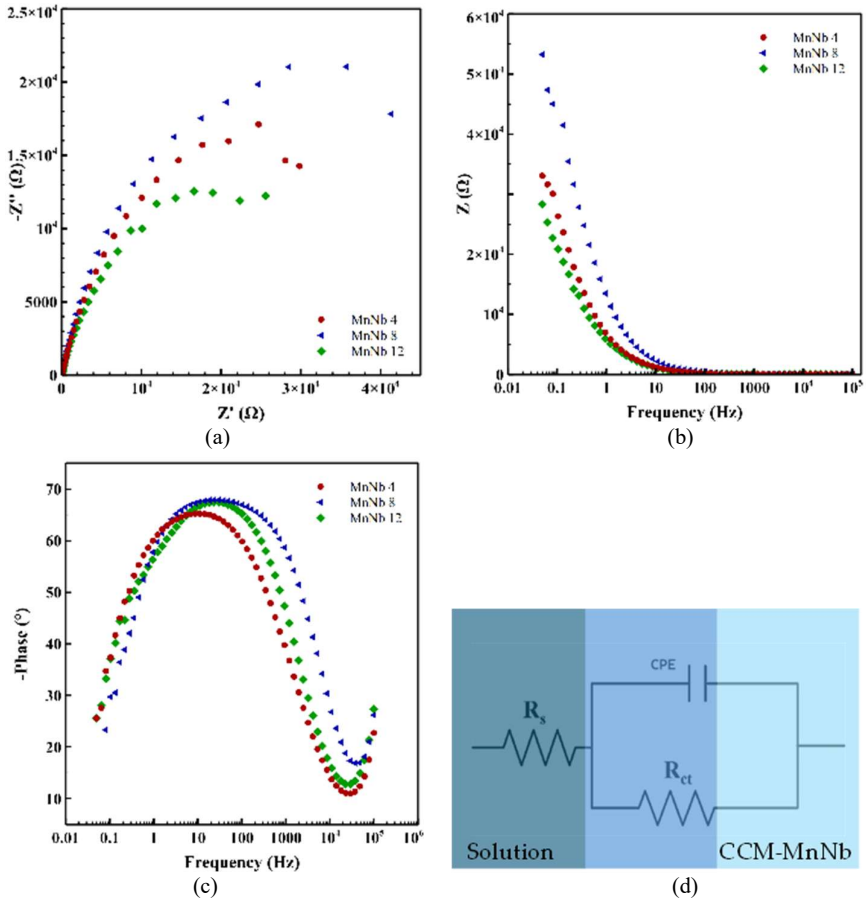

Figure 4. EIS curve of equiatomic CCM-MnNb, recorded at scan rate 1 mV/s, immersed in Hank's at 37 °C

Fig. 5 shows the Mott-Schottky plots of the CCM-MnNb alloys with different remelting cycles. The Mott-Schottky plots exhibit a positive slope; it is present that these alloys exhibit n-type semiconductive behavior. The donor densities (Nd) were approximately 3.93×10^{19} cm^{-3} (MnNb 4), 2.67×10^{19} cm^{-3} (MnNb 8), and 5.5×10^{19} cm^{-3} (MnNb 12). CCM-MnNb 8 has the lowest donor density, indicating lots of oxygen vacancies and other donor-type defects in the film structure, which means the alloys have good corrosion resistance.

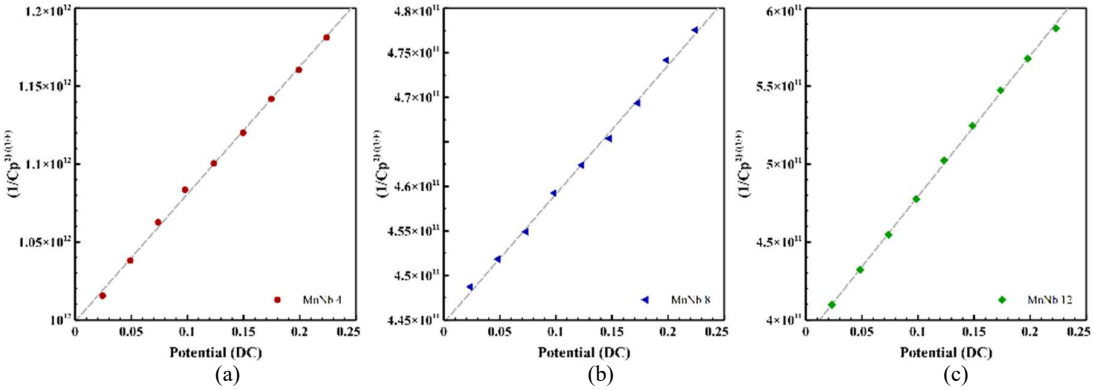

Figure 5. Mott–Schottky curve of equiatomic CCM-MnNb recorded at scan rate 1 mV/s, immersed in Hank's at 37 °C

Mn losses also affect the microstructure of CCM-MnNb, as shown in Fig. 6. The dendritic structure changed during the cycle of the remelting process. The dendrite formation in the 12-cycle remelting process is more widely distributed than in the 4- and 8-cycle processes. Besides that, the Mn losses also induce the segregation of niobium (Nb) and molybdenum (Mo) in the dendritic arm, which is indicated by the bright white area (Fig. 2). The form of dendrites in the CCM-MnNb 8 is short and tiny; it may prevent corrosion formation in the interface of the matrix and dendrite, so that it enhances the corrosion resistance of the alloys.

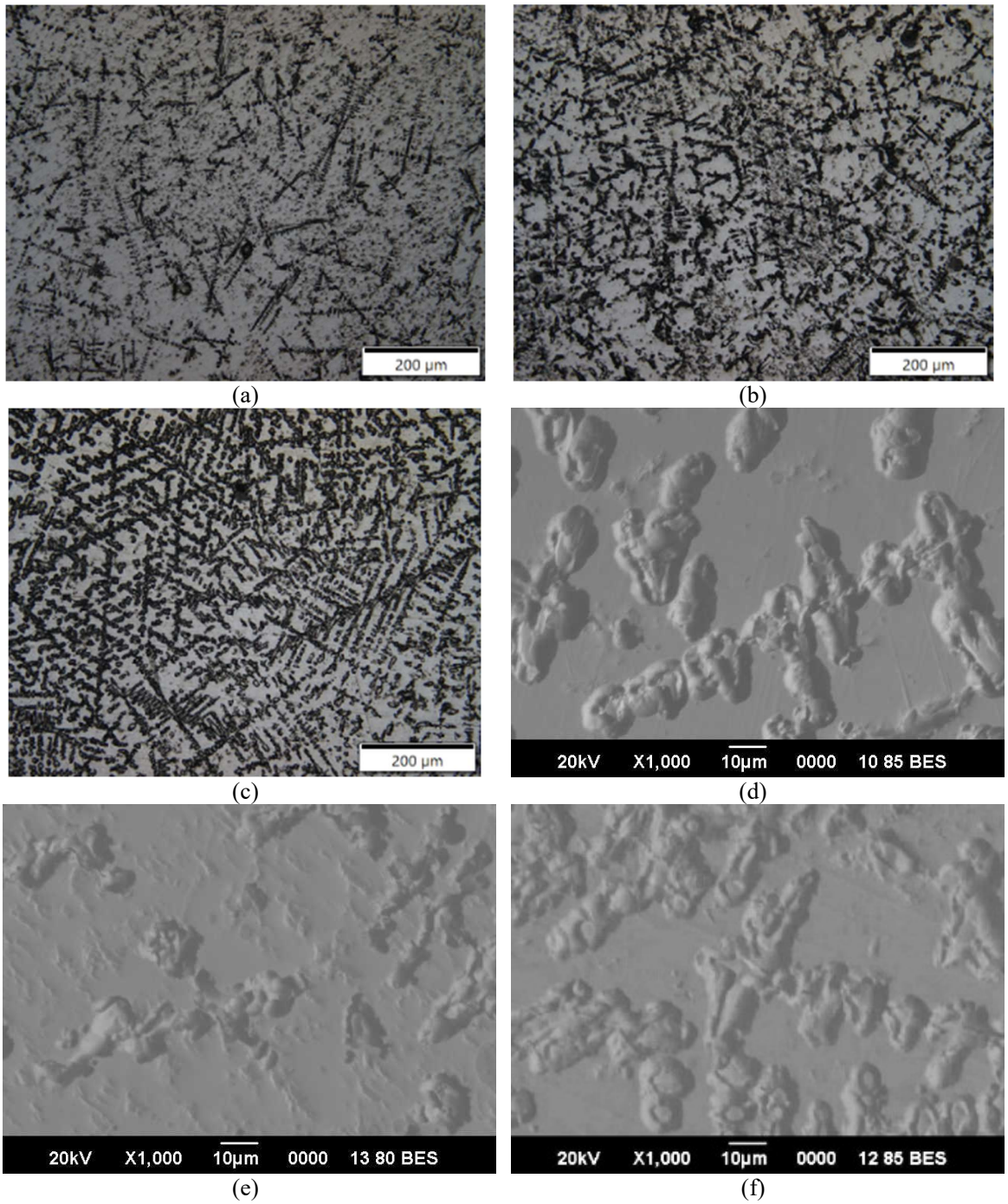

Figure 6. Microstructure of equiatomic CCM-MnNb: Optical microscope image of (a) MnNb 4, (b) MnNb 8, (c) MnNb 12; SEM-BSE image of (d) MnNb 4, (e) MnNb 8, (f) MnNb 12

The short and tiny dendrites formation in CCM-MnNb 8 induced the homogeneity of the microstructure, which significantly reduced the electrochemical potential difference between the dendrites (cathode-Mo rich) and the matrix (anode). The finer dendrite formation also reduces the surface area of the micro cathode, which can inhibit the rate of anodic solution, as confirmed by the low current density (0.619 μA/cm^2), as shown in Table 3. In addition, the finer microstructure also induced the stability of Cr_2O_3 passive film formation on the matrix surface, as indicated by the lowest donor density (2.67 × 10^{19} cm^{-3}) and highest charge transfer resistance (18,250.94 Ω/cm2) on the CCM-MnNb 8, as shown in Table 4. Comprehensively, it can prevent localized corrosion, such as pitting corrosion in the alloys, which promotes the CCM-MnNb 8 to have outstanding corrosion resistance.

Table 4. The fitting parameters of the equivalent circuit model for EIS data fitting of the CCM-MnNb alloy

	R_s	R_{ct}	Q	
	(Ω cm^{-2})	(Ω cm^{-2})	Y_0 (μFcm^{-2})	N
MnNb 4	8.94	15094.83	1.09E-05	0.23325
MnNb 8	4.91	18250.94	5.17E-06	0.24134
MnNb 12	4.54	9479.40	1.08E-05	0.21461

4. CONCLUSION

The corrosion behavior of equiatomic Bio-HEA CCM-MnNb that was fabricated through multiple remelting (4, 8, and 12 cycles) processes was investigated. The remelting process decreases Mn concentration from 20% (at. %) to 18.31% in 4 cycle times, 9.12% in 8 cycle times, and 6.7% in 12 cycle times, which is related to the homogeneity of the elemental distribution of the alloys. Furthermore, the CCM-MnNb 8 was fabricated using 8 cycles, resulting in the lowest corrosion rate (0.0038 mmpy), followed by CCM-MnNb 4 (0.0051 mmpy) and CCM-MnNb 12 (0.0053 mmpy), as well as the number of donor densities, 2.67 × 10^{19} cm^{-3}, 3.93 × 10^{19} cm^{-3}, and 5.5 × 10^{19} cm^{-3}, respectively. Nevertheless, it contrasts with the charge transfer resistance (Rct), the CCM-MnNb 8 has the highest number of 18250.94 Ω cm^{-2}, then CCM-MnNb 4 (15094.83 Ω cm^{-2}) and CCM-MnNb 12 (9479.4 Ω cm^{-2}). The CCM-MnNb 8 leads in corrosion resistance among the other equiatomic Bio-HEAs, which is attributed to the presence of the finer dendrites and the chromium oxide (Cr_2O_3) protective layer on the alloy's surface.

ACKNOWLEDGEMENT

This work was supported by the National Research and Innovation Agency (BRIN) through the Rumah Program Research Grant of Nanotechnology and Materials Research Organization (grant number 20/III.10/HK/2024). This work was also part of the Degree by Research (DbR) Program of the National Research and Innovation Agency (BRIN) of the Republic of Indonesia.

REFERENCES

[1] E. J. Pickering and N. G. Jones, "High-entropy alloys: a critical assessment of their founding principles and future prospects," *International Materials Reviews*, vol. 61, no. 3, pp. 183-202, 2016. DOI: 10.1080/09506608.2016.1180020.

[2] O. N. Senkov and D. B. Miracle, "A new thermodynamic parameter to predict formation of solid solution or intermetallic phases in high entropy alloys," *Journal of Alloys and Compounds*, vol. 658, pp. 603-607, 2016. DOI: 10.1016/j.jallcom.2015.10.279.

[3] D. B. Miracle and O. N. Senkov, "A critical review of high entropy alloys and related concepts," *Acta Materialia*, vol. 122, pp. 448-511, 2017. DOI: 10.1016/j.actamat.2016.08.081.

[4] P. Martin, C. E. Madrid-Cortes, C. Cáceres, N. Araya, C. Aguilar, and J. M. Cabrera, "HEAPS: A user-friendly tool for the design and exploration of high-entropy alloys based on semi-empirical parameters," *Computer Physics Communications*, vol. 278, p. 108398, 2022. DOI: 10.1016/j.cpc.2022.108398.

[5] B. Cantor, I. T. H. Chang, P. Knight, and A. J. B. Vincent, "Microstructural development in equiatomic multicomponent alloys," *Materials Science and Engineering: A*, vol. 375-377, no. 1-2 SPEC. ISS., pp. 213-218, 2004. DOI: 10.1016/j.msea.2003.10.257.

[6] M. Todai, T. Nagase, T. Hori, A. Matsugaki, A. Sekita, and T. Nakano, "Novel TiNbTaZrMo high-entropy alloys for metallic biomaterials," *Scripta Materialia*, vol. 129, pp. 65-68, 2017. DOI: 10.1016/j.scriptamat.2016.10.028.

[7] S. P. Wang and J. Xu, "TiZrNbTaMo high-entropy alloy designed for orthopedic implants: As-cast microstructure and mechanical properties," *Materials Science and*

DOI: 10.55981/metalurgi.2024.782

Engineering C, vol. 73, pp. 80-89, 2017. DOI: 10.1016/j.msec.2016.12.057.

[8] G. Popescu, B. Ghiban, C. A. Popescu, L. Rosu, R. Truscă, I. Carcea, V. Soare, D. Dumitrescu, I. Constantin, M. T. Olaru, and B. A. Carlan, "New TiZrNbTaFe high entropy alloy used for medical applications," *IOP Conference Series: Materials Science and Engineering*, vol. 400, no. 2, 2018. DOI: 10.1088/1757-899X/400/2/022049.

[9] T. Nagase, M. Todai, T. Hori, and T. Nakano, "Microstructure of equiatomic and non-equiatomic Ti-Nb-Ta-Zr-Mo high-entropy alloys for metallic biomaterials," *Journal of Alloys and Compounds*, vol. 753, pp. 412-421, 2018. DOI: 10.1016/j.jallcom.2018.04.082.

[10] A. Motallebzadeh, N. S. Peighambardoust, S. Sheikh, H. Murakami, S. Guo, and D. Canadinc, "Microstructural, mechanical and electrochemical characterization of TiZrTaHfNb and Ti1.5ZrTa0.5Hf0.5Nb0.5 refractory high-entropy alloys for biomedical applications," *Intermetallics*, vol. 113, p. 106572, 2019. DOI: 10.1016/j.intermet.2019.106572.

[11] T. Hori, T. Nagase, M. Todai, A. Matsugaki, and T. Nakano, "Development of non-equiatomic Ti-Nb-Ta-Zr-Mo high-entropy alloys for metallic biomaterials," *Scripta Materialia*, vol. 172, pp. 83-87, 2019. DOI: 10.1016/j.scriptamat.2019.07.011.

[12] Y. Yuan, Y. Wu, Z. Yang, X. Liang, Z. Lei, H. Huang, H. Wang, X. Liu, Ke An, and W. Wu, Z. Lu., "Formation, structure and properties of biocompatible TiZrHfNbTa high-entropy alloys," *Materials Research Letters*, vol. 7, no. 6, pp. 225-231, 2019. DOI: 10.1080/21663831.2019.1584592.

[13] T. Nagase, Y. Iijima, A. Matsugaki, K. Ameyama, and T. Nakano, "Design and fabrication of Ti–Zr-Hf-Cr-Mo and Ti-Zr-Hf-Co-Cr-Mo high-entropy alloys as metallic biomaterials," *Materials Science and Engineering C*, vol. 107, p. 110322, 2020. DOI: 10.1016/j.msec.2019.110322.

[14] J. González-Masís, J. M. Cubero-Sesin, A. Campos-Quirós, and K. Edalati, "Synthesis of biocompatible high-entropy alloy TiNbZrTaHf by high-pressure torsion," *Materials Science and Engineering: A*, vol. 825, 2021. DOI: 10.1016/j.msea.2021.141869.

[15] N. Hua, W. Wang, Q. Wang, Y. Ye, S. Lin, L. Zhang, Q. Guo, J. Brechtl, P. K. Liaw, "Mechanical, corrosion, and wear properties of biomedical Ti-Zr-Nb-Ta-Mo high entropy alloys," *Journal of Alloys and Compounds*, vol. 861, 2021. DOI: 10.1016/j.jallcom.2020.157997.

[16] T. Ishimoto, R. Ozasa, K. Nakano, M. Weinmann, C. Schnitter, M. Stenzel, A. Matsugaki, T. Nagase, T. Matsuzaka, and M. Todai, H. S. Kim, T. Nakano, "Development of TiNbTaZrMo bio-high entropy alloy (BioHEA) super-solid solution by selective laser melting, and its improved mechanical property and biocompatibility," *Scripta Materialia*, vol. 194, 2021. DOI: 10.1016/j.scriptamat.2020.113658.

[17] Y. Iijima, T. Nagase, A. Matsugaki, P. Wang, K. Ameyama, and T. Nakano, "Design and development of Ti-Zr-Hf-Nb-Ta-Mo high-entropy alloys for metallic biomaterials," *Materials and Design*, vol. 202, p. 109548, 2021. DOI: 10.1016/j.matdes.2021.109548.

[18] T. Nagase, M. Todai, and T. Nakano, "Development of Co - Cr - Mo - Fe - Mn - W and Co - Cr - Mo - Fe - Mn - W - Ag high- entropy alloys based on Co - Cr - Mo Alloys," *Materials Transactions*, vol. 61, no. 4, pp. 567-576, 2020. DOI: 10.2320/matertrans.MT-MK2019002.

[19] A. E. Bololoi, L. E. Geambazu, I. V. Antoniac, R. V. Bololoi, C. A. Manea, V. D. Cojocaru, and D. Pătroi, "Solid-state processing of CoCrMoNbTi High-entropy alloy for biomedical applications," *Materials*, vol. 16, no. 19, pp. 1-12, 2023. DOI: 10.3390/ma16196520.

[20] M. Zhang, X. Zhou, and J. Li, "Microstructure and mechanical properties of a refractory CoCrMoNbTi high-entropy alloy," *Journal of Materials Engineering and Performance*, vol. 26, no. 8, pp. 3657-3665, 2017. DOI: 10.1007/s11665-017-2799-z.

[21] F. J. Lan, C. L. Zhuang, C. R. Li, J. B. Chen, G. K. Yang, and H. J. Yao, "Study on manganese volatilization behavior of Fe-Mn-C-Al twinning-induced plasticity steel," *High Temperature Materials and Processes*, vol. 40, no. 1, pp. 461-470, 2021. DOI: 10.1515/htmp-2021-0049.

[22] Z. Zhou, Q. Wei, Q. Li, B. Jiang, Y. Chen, and Y. Sun, "Development of Co-based bulk metallic glasses as potential

biomaterials," *Materials Science and Engineering C*, vol. 69, pp. 46-51, 2016. DOI: 10.1016/j.msec.2016.05.025.

[23] W. Yang, Y. Liu, S. Pang, P. K. Liaw, and T. Zhang, "Bio-corrosion behavior and in vitro biocompatibility of equimolar TiZrHfNbTa high-entropy alloy," *Intermetallics*, vol. 124, p. 106845, 2020. DOI: 10.1016/j.intermet.2020.106845.

[24] Y. Okazaki, T. Tateishi, and Y. Ito, "Corrosion resistance of implant alloys in pseudo physiological solution and role of alloying elements in passive films," *Materials Transactions, JIM*, vol. 38, no. 1, pp. 78-84, 1997.

[25] A. W. E. Hodgson, S. Kurz, S. Virtanen, V. Fervel, C.-O. Olsson, and S. Mischler, "Passive and transpassive behaviour of CoCrMo in simulated biological solutions," *Electrochimica Acta*, vol. 49, no. 13, pp. 2167-2178, 2004.

[26] A. Ghiban, B. Ghiban, C. M. Bortun, and M. Buzatu, "Structural investigations in CoCrMo (Ti) welded dental alloys," *Rev. Chim. (Bucharest)*, vol. 65, no. 11, pp. 1314-1318, 2014.

[27] D. Kuroda, M. Niinomi, M. Morinaga, Y. Kato, and T. Yashiro, "Design and mechanical properties of new β type titanium alloys for implant materials," *Materials Science and Engineering: A*, vol. 243, no. 1-2, pp. 244-249, 1998. DOI: 10.1016/s0921-5093(97)00808-3.

[28] X. Z. Wang, Q. Hu, L. Zhang, and Z. Cui, "The influence of Nb addition on the passivity of CoCrNiNbx multi-principal element alloys," *Journal of Electroanalytical Chemistry*, vol. 908, 2022. DOI: 10.1016/j.jelechem.2022.116107.